Peer-reviewed version available at *Water* **2017**, *9*, 100; doi:10.3390/w9020100

Article

Modeling Glacier Mass Balance and Runoff in the Koxkar River Basin on the South Slope of the Tianshan Mts. during 1959 to 2009, China

Min Xu [1], Haidong Han [2] and Shichang Kang [1,*]

[1] State Key Laboratory of Cryospheric Science, Cold and Arid Regions Environmental and Engineering Research Institute, Chinese Academy of Sciences, Lanzhou 730000, China; xumin@126.com

[2] CAS Center for Excellence in Tibetan Plateau Earth Sciences, Chinese Academy of Sciences, Beijing 100101, China; hhd@lzb.ac.cn

* Correspondence: shichang.kang@lzb.ac.cn; Tel.: +86-931-496-7368

Abstract: Water resources provided by alpine glaciers are an important pillar for people living in the arid regions in the west of China. In this study, the HBV (Hydrologiska Byrans Vattenavdelning) light model was applied to simulate glacier mass balance and runoff in the Koxkar River Basin (KRB) on the south slope of Mt. Tumur, western Tianshan Mts.. Daily temperature and precipitation were calculated by multiple linear regressions and gradient-inverse distance weighting, respectively, based on in-situ observed data by automatic weather stations (AWSs) in the basin (2007–2009) and at four meteorological stations neighbering the basin (1959–2009). Observed daily air temperature and precipitation were taken as input data for the HBV model, which was calibrated using runoff in 2007/08 and 2009/10, and validated in 2008/09 and 2010/11. Generally, the model could simulate runoff very well. The annual glacier mass balance and runoff were calculated using the HBV model driven by interpolated meteorological data for the period of 1959–2009. The simulated glacier mass balance were reasonable when compared with those observed values at nearby glaciers, indicating a decrease trend of mass balance in the basin with an average value of –370.4 mm a^{-1} since 1959. The annual runoff showed a slight increase trend (5.51 mm a^{-1}). Futher analysis indicated that the runoff is more sensitive to temperature than precipitation amuont in the Koxkar river basin.

Keywords: glacier mass balance; runoff; Tianshan Mts.; Koxkar River Basin; HBV model; interpolation

1. Introduction

Glaciers concentrated in mountain regions are important water resources and an oasis of economic lifeblood in arid and semi-arid areas in western China [1-3]. Rising temperatures have resulted in the loss of more than half of the glacier volume in Asia since 1900 [4]. In the northwestern arid area of China, the importance of meltwater is particularly prominent, meltwater runoff accounts for 22% of the runoff from mountains.and glacier meltwater from Tianshan Mts. supplies 38.5% of the total runoff in the Tarim River basin [5]. Since 1980s, streamflow significantly increase which flow out from Tianshan Mts., the retreat of glaciers has a major impact on water resources in arid regions [6].

Hydrology in the arid region has become an important topic of research [7]and hydrological model can simulate hydrological processes and is of great practical significance

Peer-reviewed version available at Water 2017, 9, 100; doi:10.3390/w9020100

and scientific value for exploring new ideas about integrated river basin management of water resources [8]. However, due to the extremely high altitude and difficult environment of the Tianshan Mts., hydro-meteorological data for this inaccessible area are rare, especially in the glaciated watersheds. Additionally, there has been few application of hydrological models to the south slope of Mt. Tumur, Tianshan Mts.. Therefore, it is urgent to investigate water resources from glaciers in this area.

The HBV (Hydrologiska Byrans Vattenavdelning) model was developed by the Swedish Meteorological and Hydrological Institute (SMHI) for the cold regions in 1973. The HBV model, with its strong practical aspects and improved simulation results, has been applied successfully to forecast runoff for more than 200 river basins in Sweden and has been successfully applied in more than 40 countries of the world to study hydrological processes under climate change, changes of permafrost, and changes of land use [9-14]. The HBV model is a semi-distributed conceptual model that requires less data input and produces better simulation results [15]. It has also been successfully used in different watersheds in the cold region of western China. Kang et al. (2002) established a conceptual hydrological model for upstream of Hei river in Qilian Mts. of western China based on the principle of the HBV model. The model is in accordance with the characteristics of formation of mountain runoff in study area, where the basin was divided into two basic landscape zones, alpine tundra-snow and mountain vegetation, and the simulation were well [16]. In addition, the model has applicability to glaciated watersheds in the Tibetan Plateau, where it also achieved well, the HBV light model includes glacier module which is more applicable for mountain regions where glacier distributed [17].

In this study, the HBV light model and the principle of water balance were employed to simulate the change in runoff depth, evaporation, glacier mass balance (GMB), and glacier runoff in the Koxkar river basin (KRB) during 1959 to 2009. The work aims to reconstruct climate change in the past 50 years in the region, to understand changes in glacier mass balance and runoff in response to climate change. This work may provide knowledge for water resource management in the arid regions of central Asia.

2. Study Area and Data collecting

2.1 Study Area

The KRB is located in the southern Mt. Tumur, western Tianshan Mts., and is one of the source regions of the Akesu river (Fig. 1). The KRB has a total area of 116.5 km^2 with glacier area of 89.6 km^2 (76.9%), and its elevation ranges from 2960 to 6342 m a.s.l.. The length of Koxkar glacier is 25.1 km, and the ice volume is 15.79 km^3. Annual precipitation is about 533 mm in the KRB which is supplied mainly by moisture from the Atlantic and Arctic. Of the precipitation, 50% occurs from June to August, 70% occurs from May to September, and about 30% occurs during the cold season. Annual precipitation near the snow line is 750–850 mm [18-20]. There are one automatic weather station (AWS) and one hydrological station located in the terminal of the glacier (Base Camp) (2974 m a.s.l.) (Fig. 1), and other four AWSs located in the glacier with elevations of 3200, 3400, 3700, and 4200 m a.s.l., respectively (Fig. 1).

doi:10.20944/preprints201610.0139.v1

Peer-reviewed version available at *Water* **2017**, *9*, 100; doi:10.3390/w9020100

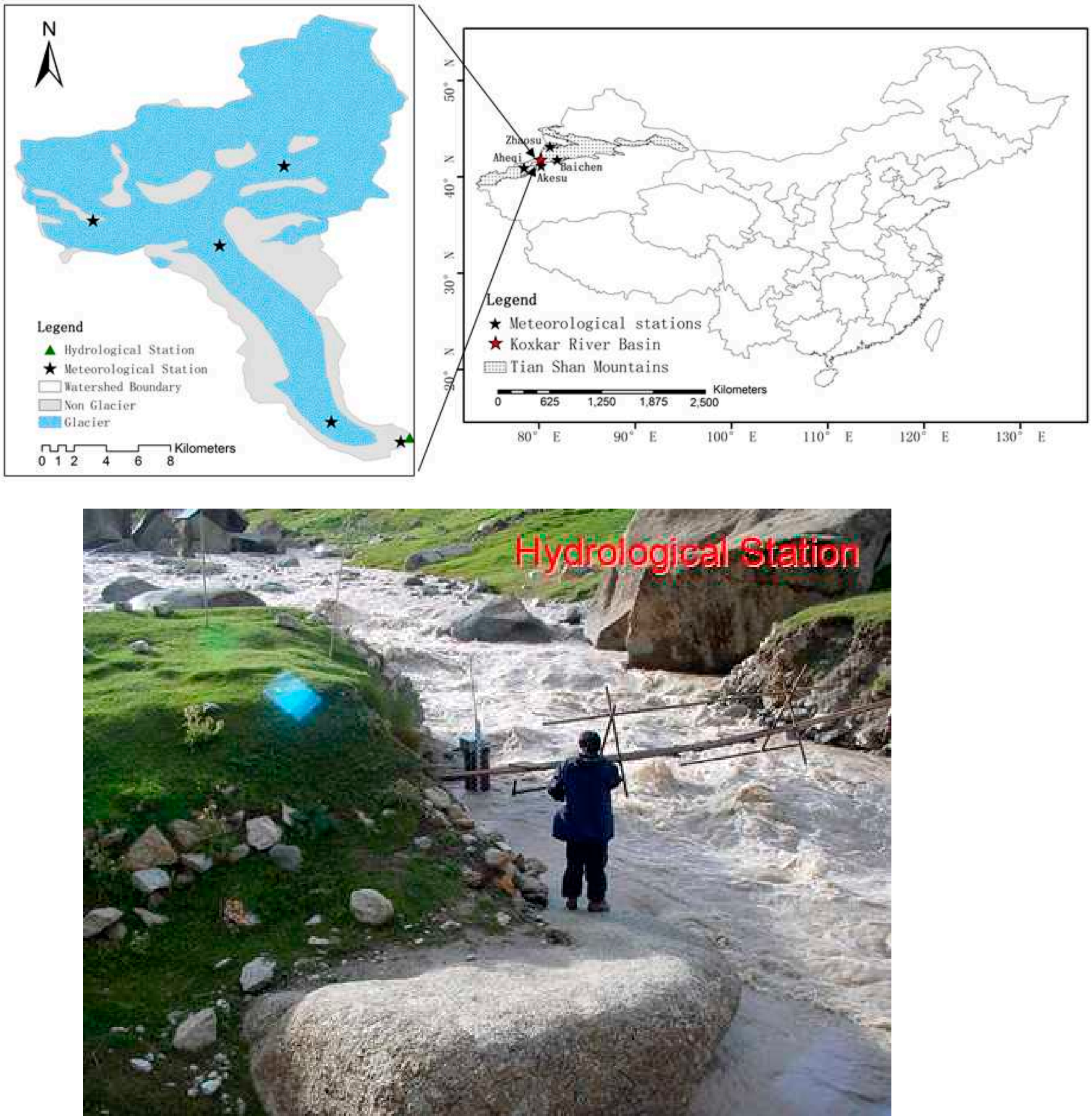

Fig. 1 Locations of the Koxkar glacier and observation sites areas. Four meteorological stations around the Koxkar river basin are shown at top right

2.2 Geographical data

The HBV light model requires geographical data including digital elevation model (DEM), aspect, and land cover. The 30-m-resolution Global DEM (http://datamirror.csdb.cn) and a digital vector map of modern glaciers were obtained from the Chinese Glacier Inventory [20]. The basin was divided by altitude zones, aspect zones, and zones with and without glacier (Fig. 2). The land cover data were taken from the Science Data Center for Cold and Arid Regions (http://westdc.westgis.ac.cn/). The land cover types include bare land, shrub, grassland, snow cover, glacier, and water (Table. 1).

Preprints (www.preprints.org) | NOT PEER-REVIEWED | Posted: 31 October 2016 doi:10.20944/preprints201610.0139.v1

Peer-reviewed version available at Water 2017, 9, 100; doi:10.3390/w9020100

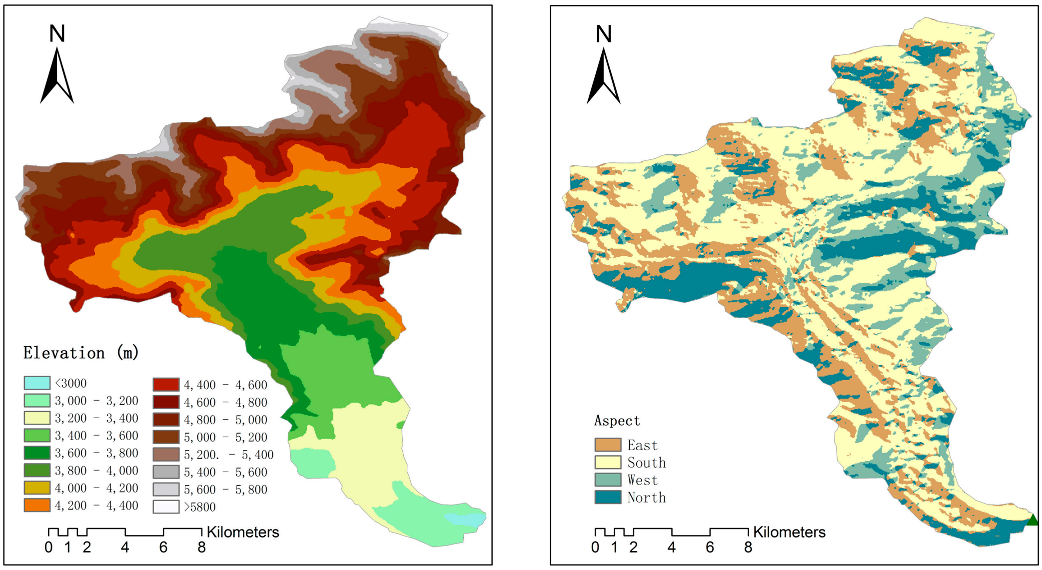

Fig. 2 Elevation and aspect in the Koxkar river basin

Table 1 Types of vegetation in the

Cover type	Area (km²)	Proportion
Bare Land	9.3	8.0%
Shrub	1.8	1.5%
Grassland	6.15	5.3%
Snow Cover	6.9	5.9%
Glacier	89.6	76.9%
Water	2.7	2.32%

2.3 Observations and meteorological data

The HBV light model requires data of daily air temperature and precipitation, and thire gradients. Five AWSs were established in the KRB in 2007 and have operated until present (Fig. 1). Precipitation was monitored by both manual rain gauge and automatic snow/rain gauge (T-200B weighting rain gauge). This study used air temperature and precipitation from the AWS at the Base Camp (Camp-AWS) as the input data due to the higher quality. Based on the altitudes of the five AWSs, we calculated the temperature and precipitation gradients as 0.66℃ (100 m)$^{-1}$ and 4.6% (100 m)$^{-1}$, respectively. Since meteorological observations started in 2007; in the KRB, the long-term air temperature and precipitation (1959 - 2009) were reconstructed using data recorded at four national meteorological stations (NMSs) (Fig. 1, Table. 2) (for the method see section 4) neighbering the basin.

Table. 2 Details of the Camp-AWS and the four national meteorology stations (NMS) around the Koxkar river basin

Station	Longitude (°E)	Latitude (°N)	Altitude (m)	Year
Akesu	80.233	41.167	1103	1959-2009
Baichen	81.900	41.783	1229	1959-2009
Aheqi	78.450	40.930	1985	1959-2009
Zhaosu	81.133	43.150	1851	1959-2009
Koxkar	80.167	41.700	2974	2007-2009

2.4 Hydrological and glacial data

Hydroligical station was established in 2007 at the base camp (BC) (Fig. 1). Water stage has been measured by automatic HOBO meter with an interval of 30 mins and flow velocity was measured manually by hydrodynamometer. Through several measurements at different water stages, the relationship between water stage and discharge was established. Then, the discharge were calculated at the BC from 2007 to 2011.

3. HBV Model

The HBV model is a semi-distributed model, which means that a catchment can be separated into different elevation and vegetation zones as well as into different subcatchments [22]. The HBV light conceptual runoff model, as presented here, is based on the HBV model [23]. It was coupled with a more detailed snow and glacier melt subroutine employing the degree-day approach [24]. The subroutine has a physical basis. For this study, the HBV light model, which takes into account various aspect classes in each elevation belt and couples Monte Carlo and genetic algorithms to calibrate the parameters automatically [25, 26], was applied to model runoff depth, glacier runoff, and GMB in the KRB. The model is composed mainly of the input data, which were processed semi-distributed by four modules: the glacier ablation module, soil module, response module, and flow concentration module (Fig. 3)[22].

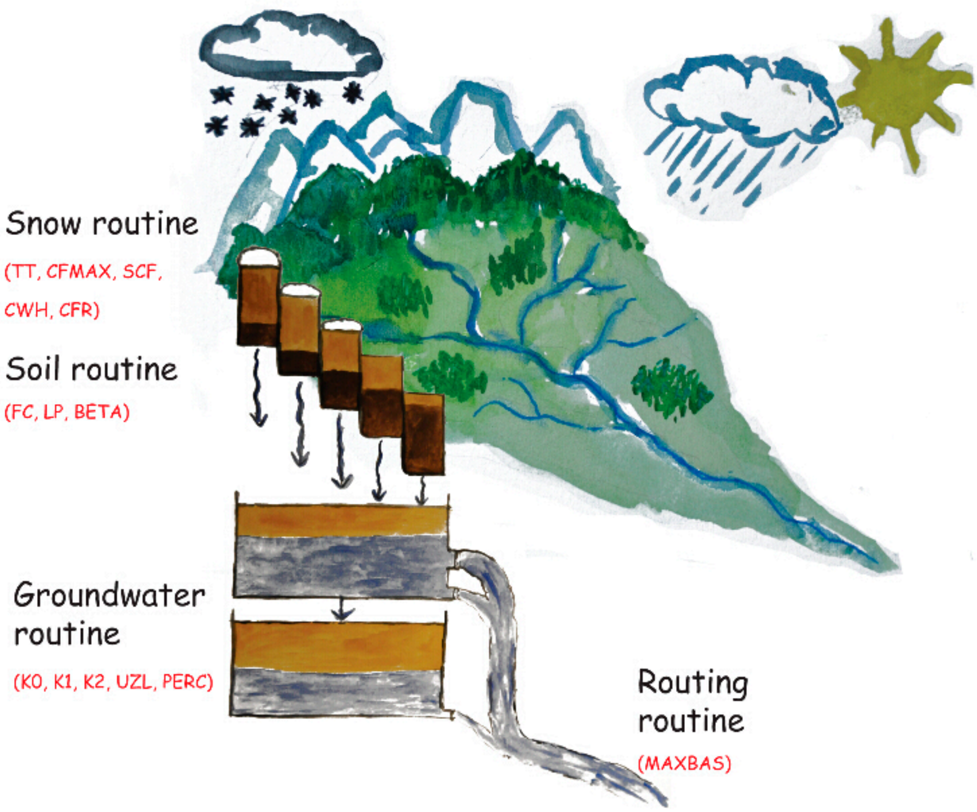

Fig. 3 Schematic structure of the HBV light model

The main formulae of each module are described as follows. The model simulates daily discharge using daily rainfall and temperature as input. Precipitation is simulated to be either snow or rain depending on whether the temperature is above or below a threshold temperature, *TT* [℃]. All precipitation simulated to be snow, i.e., falling when the temperature is below *TT*, is multiplied by a snowfall correction factor, *SFCF*. In the snow and glacier routine, the amount of meltwater is calculated by the degree-day method [27], which uses positive degree days (while daily mean temperature is above 0 ℃) multiplied by a factor. This model also considers the influence of different aspect and different melt intensity of glacier and snow [25](Eq. 2). Meltwater and rainfall are retained within the snowpack until the amount exceeds a certain fraction, *CWH*, of the water equivalent of the snow. Refreezing of meltwater is also considered in this model [28-30]. Liquid water within the snowpack refreezes according to Eq. 3. Rainfall and snowmelt (P) are divided into water filling the soil box and groundwater recharge depending on the relation between water content of the soil box (*SM* [mm]) and its largest value (*FC* [mm]) (Eq. 4). Actual evaporation from the soil box equals the potential evaporation if *SM*/*FC* is above *LP*, whereas a linear reduction is used when *SM*/*FC* is below *LP* (Eq. 5) (Bergström 1973). Groundwater recharge is added to the upper groundwater box (SUZ [mm]). *PERC* [mm d^{-1}] defines the maximum percolation rate from the upper to the lower groundwater box (*SLZ* [mm]). Runoff from the groundwater boxes is computed as the sum of two or three linear outflow equations depending on whether or not *SUZ* is above a threshold value, *UZL* [mm] (Eq. 6). This runoff is finally transformed by a triangular weighting function defined by the parameter *MAXBAS* (Eq. 7) to give the simulated runoff [mm d^{-1}]. If different elevation zones are used, the changes in precipitation and temperature with elevation are calculated using the two parameters *PCALT* [%/100 m]

Preprints (www.preprints.org) | NOT PEER-REVIEWED | Posted: 31 October 2016 doi:10.20944/preprints201610.0139.v1

Peer-reviewed version available at Water 2017, 9, 100; doi:10.3390/w9020100

and *TCALT* [ºC/100 m] (Eqs. 8 and 9). The long-term mean of the potential evaporation, *Epot, M,* for a certain day of the year can be corrected to its value at day *t*, *Epot(t)*, by using the deviations of the temperature, *T(t)*, from its long-term mean, *TM*, and a correction factor, *CET* [°C-1] (Eq. 10) [31, 32].

$$P_L(h) = P_t(h) \quad T_t(h) > TT; \qquad P_S(h) = P_t(h) \cdot SFCF \quad T_t(h) < TT \tag{1}$$

$$melt = CFMAX\,(T\,(t) - TT) \tag{2}$$

$$refreezing = CFRC\ FMAX\,(TT - T(t)) \tag{3}$$

$$\frac{recharge}{P(t)} = \left(\frac{SM(t)}{FC}\right)^{BETA} \tag{4}$$

$$E_{act} = E_{pot}\ min\,(\frac{SM\,(t)}{FC \cdot LP}, 1) \tag{5}$$

$$Q_{GW}(t) = K_2 SLZ + K_1 SUZ + K_0 max\,(SUZ - UZL, 0) \tag{6}$$

$$\begin{aligned} Q_{sim}(t) &= \sum_{i=1}^{MAXBAS} c\,(i)\ QGW\,(t - i + 1) \\ where\ c\,(i) &= \int_{i-1}^{i} \frac{2}{MAXBAS} - \left| u - \frac{MAXBAS}{2} \right| \frac{4}{MAXBAS^2} du \end{aligned} \tag{7}$$

$$P\,(h) = P_0(1 + \frac{PCALT\,(h - h_0)}{10000}) \tag{8}$$

$$T\,(h) = T0 - \frac{TCALT\,(h - h_0)}{100} \tag{9}$$

$$\begin{aligned} &E_{pot}(t) = (1 + C_{ET}(T\,(t) - T_M)\,)\,E_{pot,\ M} \\ &but\ \ 0 \le E_{pot}(t) \le 2E_{pot,\ M} \end{aligned} \tag{10}$$

The R_{eff} and the coefficient of determination (r^2) are used for assessment of simulations [33]. The formulae are as follows (Eqs 11 and 12).

$$R_{eff} = 1 - \frac{\sum(Q_{Sim}(t) - Q_{Obs}(t))^2}{\sum(Q_{Obs}(t) - \overline{Q_{Obs}})^2} \tag{11}$$

$$r^2 = \frac{(\sum(Q_{obs} - \overline{Q_{obs}})(Q_{sim} - \overline{Q_{sim}}))^2}{\sum(Q_{obs} - \overline{Q_{obs}})^2 \sum(Q_{sim} - \overline{Q_{sim}})^2} \tag{12}$$

Preprints (www.preprints.org) | NOT PEER-REVIEWED | Posted: 31 October 2016 doi:10.20944/preprints201610.0139.v1
Peer-reviewed version available at Water 2017, 9, 100; doi:10.3390/w9020100

4. Reconstruction of temperature and precipitation data

Undstanding the climate, discharge, and GMB in past decades is important for predicting future trends. In this work, we used the HBV hydrological model to simulate runoff and GMB from 1959 to 2009. Long-term observed data are unavailable for the basin, so it was necessary to reconstruct the historical runoff and GMB. The daily air temperature and precipitation in the KRB were reconstructed for the period 1959–2009 based on in-situ meteorological observations in the KRB during 2007–2009 and those from the four NWSs around the KRB during 1959–2009.

4.1 Reconstruction of temperature

There are many methods to interpolate temperature, e.g., inverse distance weight, trend surface, kriging interpolation, cokring interpolation, and these methods are usually used to interpolate the spatial distribution of temperature. However, they require a high number of data points for calculation. In this study, we had only four NMSs for interpolation (Table 2). Thus, the previous temperature data were interpolated by the statistical method of multiple regression analysis, which depended only on the temperature recorded at the four stations. Two equations were formulated because the four stations had records of various length.

$$T_0 = 0.3098 \times T_1 - 0.2314 \times T_2 - 0.0304 \times T_3 + 0.7211 \times T_4,\ R^2 = 0.942 \quad (13)$$

$$T_0 = 1.2292 \times T_1 - 0.3211 \times T_2 - 0.1725 \times T_3,\ R^2 = 0.918 \quad (14)$$

T_0 is the daily air temperature at Camp-AWS and T_1, T_2, T_3, and T_4 are the daily air temperatures of Akesu, Baichen, Aheqi, and Zhaosu, respectively. The result calculated by Eq. (13) ($R^2 = 0.942$) was better than that calculated by Eq. (14) ($R^2 = 0.918$), so we used Eq. (13) to reconstruct the daily temperature. The reconstructed daily temperatures fit well to the observation ones from 2007 to 2009 ($R^2 = 0.91$; $p < 0.01$) (Fig. 4). The temperature increased 0.32 ℃ ($10a^{-1}$) ($p < 0.01$) in the past semi-century in the KRB, which is a little higher than the average change in the southern slope of the Tianshan Mts. (0.30 ℃ ($10a^{-1}$)) [34].

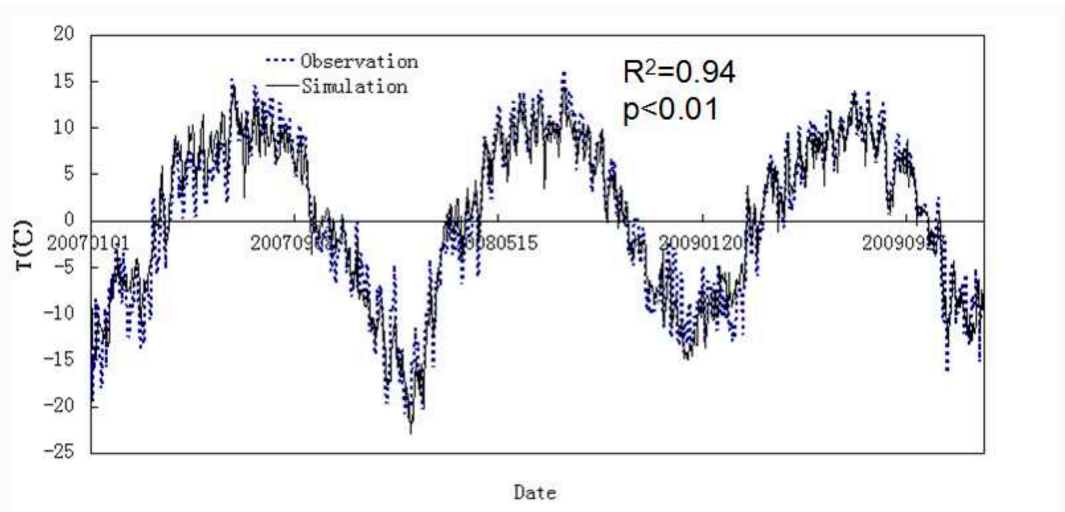

Fig. 4 Comparison of simulated and observed daily temperature at Camp-AWS from 2007 to 2009

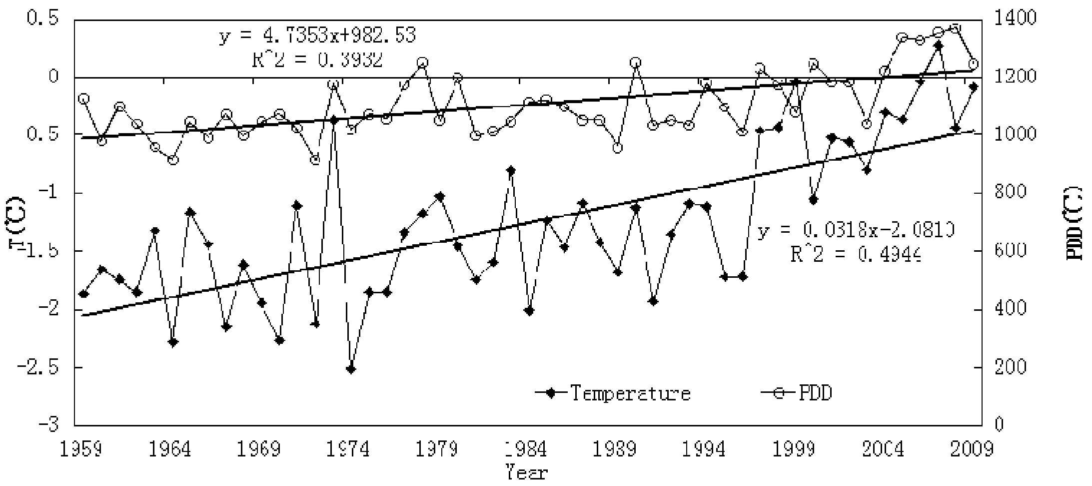

Fig. 5 Reconstructed yearly average air temperature (T) and positive degree-days (PDD) at Camp-AWS during 1959–2009

4.2 Reconstruction of precipitation

The precipitation, which has large temporal variation, was influenced by the terrain in the Tianshan Mts.. The reconstruction of precipitation was conducted as follows. We used stepwise multiple regression analysis to eliminate stations that recorded precipitation farther from the Camp-AWS precipitation in a step-by–step manner. Stations were eliminated in the order of Akesu, Baichen, Aheqi, and Zhaosu, respectively. The correlation between Camp-AWS and Akesu was not significant due to Akesu located in the low land city. Therefore, we used date from other three stations located in the mountain regions to interpolate the Camp-AWS precipitation.

The precipitation gradient and inverse distance weighting (IDW) methods were combined to reconstruct Camp-AWS precipitation from 1959 to 2009. The gradients of precipitation were 2.05 mm/100 m, 3.54 mm/100 m, and 1.6 mm/100 m between Camp-AWS and Baichen, Aheqi, and Zhaosu, respectively, from 2007 to 2009. Based on the three precipitation gradients, we calculated the precipitations at the same elevation as Camp-AWS from 1959 to 2009, respectively. Then, we used IDW to calculate the precipitation at Camp-AWS from 1959 to 2009 (Eq. 15).

$$P_0 = \frac{S_1}{S_1+S_2+S_3} * \frac{P_{0\,annual}}{P_{1\,annual}} * P_1 + \frac{S_2}{S_1+S_2+S_3} * \frac{P_{0\,annual}}{P_{2\,annual}} * P_2 + \frac{S_3}{S_1+S_2+S_3} * \frac{P_{0\,annual}}{P_{3\,annual}} * P_3 \quad (15)$$

In Eq. (15), P_0 is the daily precipitation of Camp-AWS and P_1, P_2, and P_3 are the daily precipitation of the NMSs at Baichen, Aheqi, and Zhaosu, respectively. $P_{0\,annual}$, $P_{1\,annual}$, $P_{2\,annual}$, and $P_{3\,annual}$ are the average annual precipitation of Camp-AWS, Baichen, Aheqi, and Zhaosu, respectively, during 2007 to 2009. S_1, S_2, and S_3 are the distances between Camp-AWS and Baichen, Aheqi, and Zhaosu, respectively.

Comparison of reconstructed with observed monthly precipitation is shown in Fig. 6 (R^2 reached 0.91; $p < 0.01$). Because precipitation is very important for the simulation of runoff and GMB, we needed to obtain a more vigorous validation for the reconstructed result. Thus,

Preprints (www.preprints.org) | NOT PEER-REVIEWED | Posted: 31 October 2016 doi:10.20944/preprints201610.0139.v1

Peer-reviewed version available at Water 2017, 9, 100; doi:10.3390/w9020100

the coefficient of efficiency (R_{eff}) (Eq. 11) was used to evaluate the reconstructed daily result. R_{eff} was 0.88 from 2007 to 2009 which is fairly satisfactory considering the great varying of precipitation in the mountainous regions. By applying the above method, the annual precipitation at Camp-AWS from 1959 to 2009 was reconstructed (Fig. 7). The precipitation increased by 4.8 mm a^{-1} ($p < 0.05$), consistent with those of other studies [34].

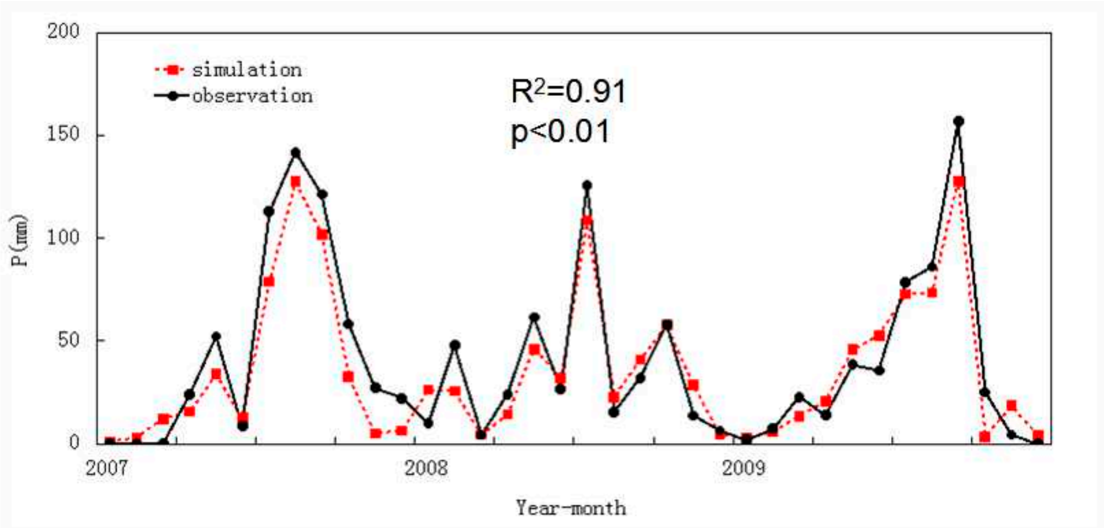

Fig. 6 Comparison of simulated and observed monthly precipitation (P) at Camp-AWS from 2007 to 2009

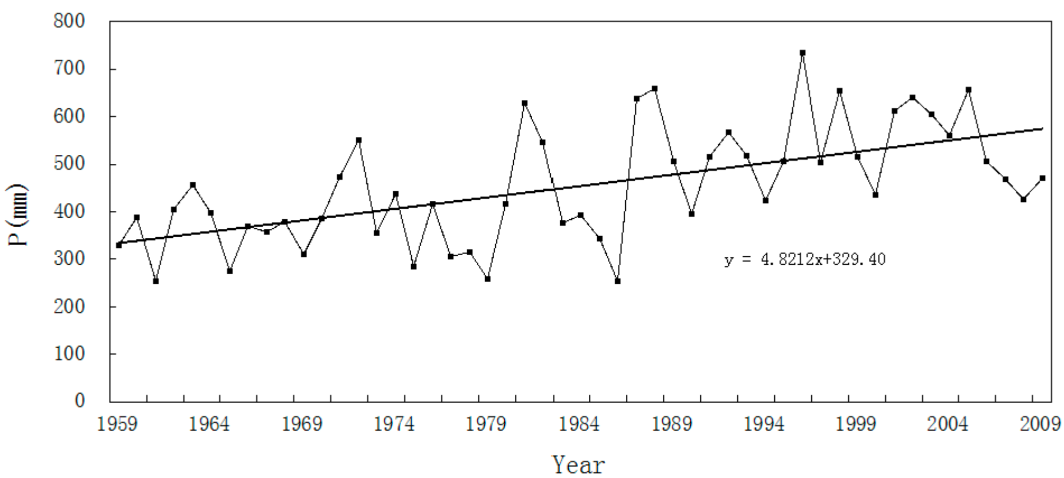

Fig. 7 Reconstructed yearly average precipitation (P) at Camp-AWS during 1959–2009

5. Results and discussion

5.1 Model calibration and validation

Except for meteorological data, there are 13 parameters in the HBV model that need to be calibrated (Table 3). To obtain a proper set of parameters, we gave every parameter a reasonable range according to the literature. A set of parameters representing the

Peer-reviewed version available at Water 2017, 9, 100; doi:10.3390/w9020100

characteristics of the KRB was then automatically obtained by employing the Monte Carlo method [35-37]. We selected hydrological data from 2007/08 and 2009/10 for calibration. In addition, data for 2008/09 and 2010/11 were used for validation.

Table 3 Definition of and set of optimized parameters of HBV for the Koxkar river basin

Parameter	*Description*	*Unit*	*Range*	*Value*	*Method of estimation*
Meteorological data					
PC_{alt}	Gradient of precipitation	%/100m	4.6	4.6	Observation
TC_{alt}	Gradient of temperature	℃/100m	0.66	0.66	Observation
Snow and glacier routine					
TT	Threshold temperature	℃	-1-2.7	2.7	(He et al. 2009)
DDF	Degree-day factor of snow	mm℃$^{-1}$day^{-1}	9.5	9.5	Observation
CFR	Refreezing coefficient	-	0.2	0.2	(Fujita et al. 2007) & Calibration
SFCF	Snowfall correction factor		0-1	0.05	
C_g	Factor for increased melt of ice	-	1.3	1.3	(Zhang et al. 2005) & Calibration
C_a	Factor for increased melt of south slope to north slope	-	1.1-2	1.1	Calibration
Soil routine					
FC	Maximum SM	mm	100-450	300	(Seibert 1997) & Calibration
LP	SM threshold for reduction of evaporation	-	0.3-0.1	0.9	(Seibert 1997) & Calibration
BETA	Shape coefficient	-	1-5	1.5	(Seibert 1997) & Calibration
Response routine					
K_1	Recession coefficient	day^{-1}	0.01-0.2	0.01	(Seibert 1997) & Calibration

Peer-reviewed version available at Water 2017, 9, 100; doi:10.3390/w9020100

K_2	Recession coefficient	day^{-1}	0.001-0.1	0.05	(Seibert 1997) & Calibration
PERC	Maximal flow from upper to lower GW-box	mm day^{-1}	0-6	2	(Seibert 1997) & Calibration
Routing routine					
MAXBAS	Routing, length of weighting function	day	1-5	1.9	(Seibert 1997) & Calibration

For the calibration period, R_{eff} and R^2 are 0.76 and 0.76 for 2007/2008, and 0.90 and 0.89 for 2009/2010, respectively. For the validation period, R_{eff} and R^2 are 0.85 and 0.86 for 2008/2009 and 0.78 and 0.81 for 2010/2011, respectively (Fig. 8). The results are acceptable on the daily scale, especially considering the uncertainty in both observation and simulation data in such a mountainous area. The modeling result reflects the actual runoff well. All R_{eff} values of the daily runoff are greater than 0.76. R_{eff} is even better (0.94) for the monthly result (Fig. 9), and there is only a 6% difference between the observed and simulated annual runoff. Considering the dominant role of glacier runoff in the KRB, the reason for the above differences may be that increasing the temporal resolution of simulated runoff led to decreases in the accuracy of the degree-day model [38].

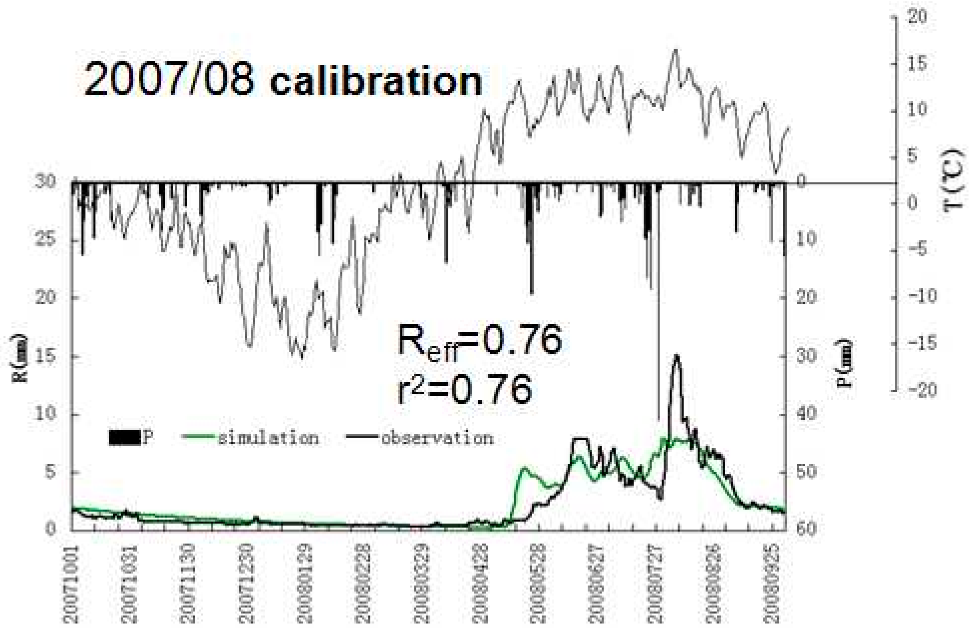

Peer-reviewed version available at Water 2017, 9, 100; doi:10.3390/w9020100

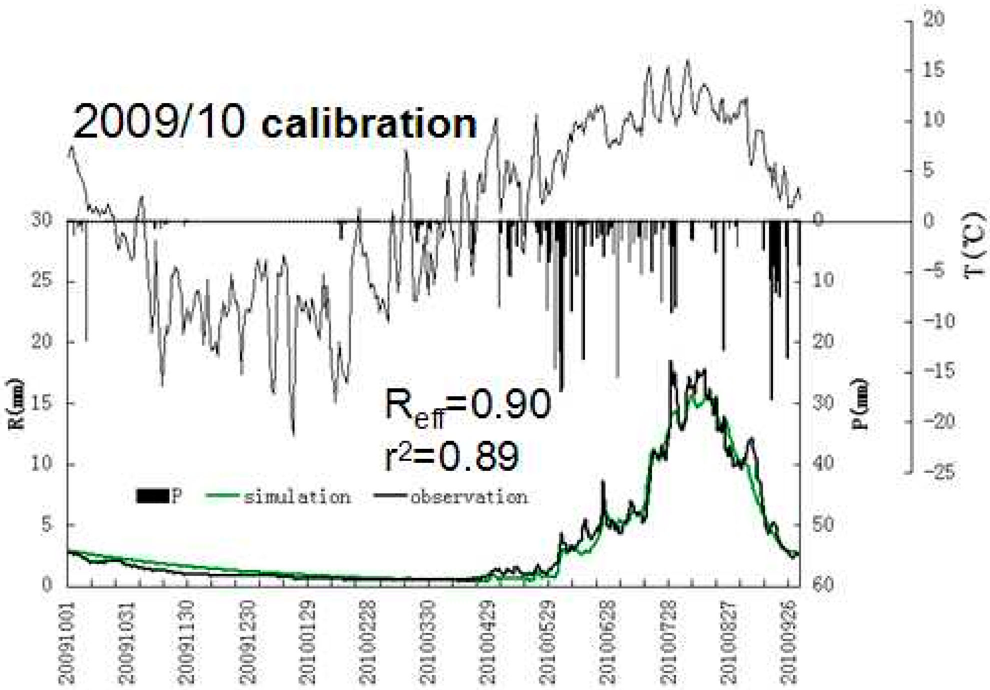

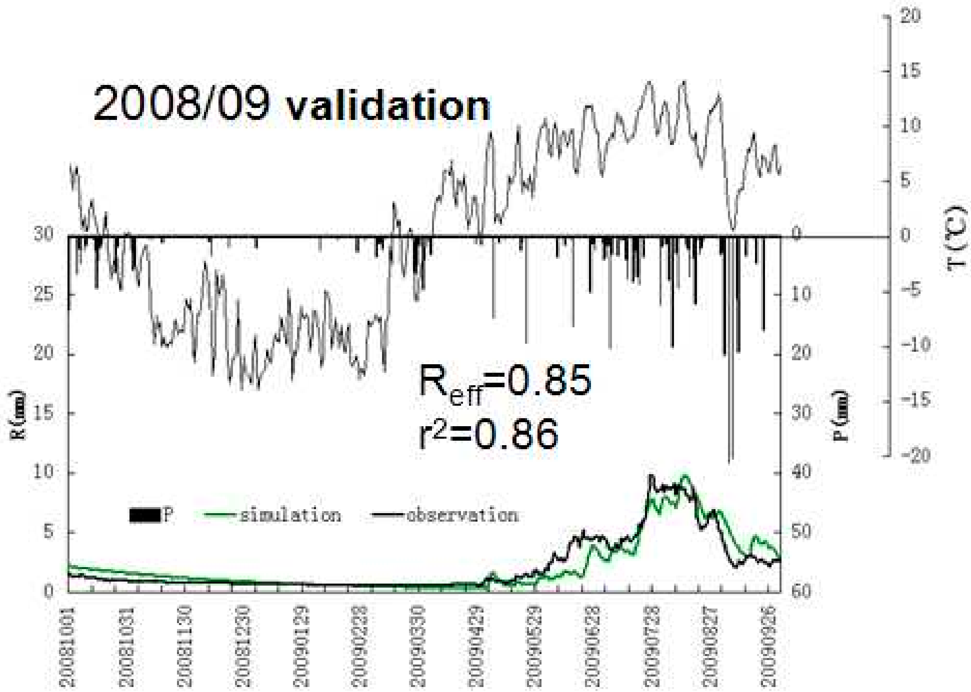

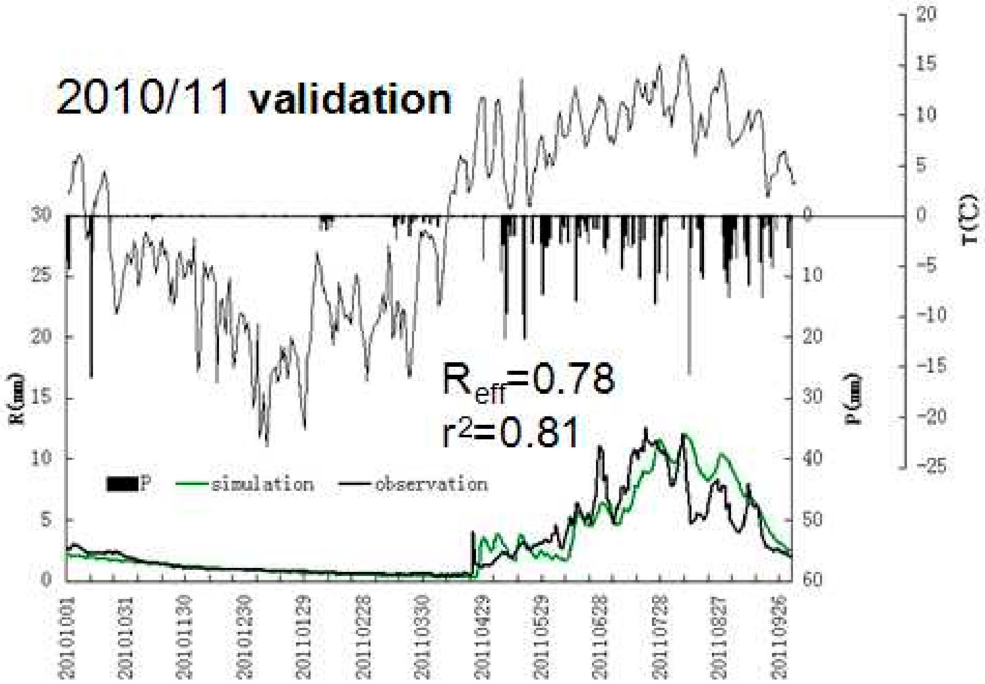

Fig. 8 Observed precipitation, temperature, and discharge and discharge generated by the HBV model during 2007/08–2010/11 (calibration periods: 2007/08, 2009/10; validation periods: 2008/09, 2010/11)

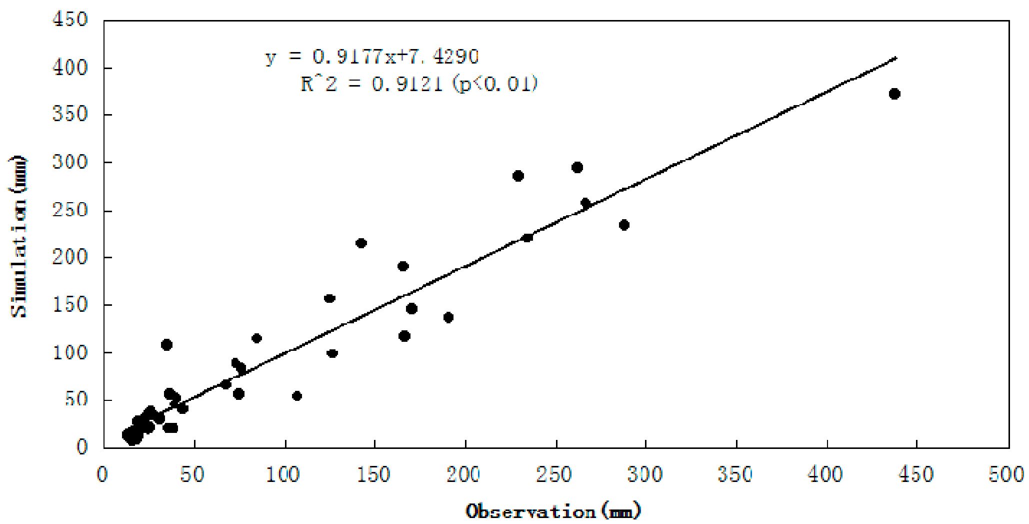

Fig. 9 Comparison of monthly simulated (R_{sim}) and observed runoff depth (R_{obs}) from 2007 to 2011

5.2 Simulation of runoff and GMB for 1959–2009

We assumed that the set of parameters did not change from 1959 to 2009, and the runoff depth and evaporation were simulated (Fig. 6(a), (b)) using the reconstructed data. The runoff depth increased 5.5 mm a^{-1} ($p < 0.01$), and it increased more significantly after the 1990s than before the 1990s. The simulated result is consistent with the results for other watersheds in which runoff is observed in the Tianshan Mts. [39]. Evaporation increased by 3.5 mm a^{-1} in the KRB. On the basis of the water balance principle (Eq. (16)), the change in water volume in the basin (ΔS) equals the total precipitation (P) minus the runoff (R), soil evaporation and sublimation (E_s), and evaporation at the glacier surface (E_g).

$$\Delta S = P - R - E_s - E_g \quad (16)$$

$$\Delta S = \Delta S_s + B \quad (17)$$

$$B = P - R - E_s - E_g \quad (18)$$

ΔS is the sum of the soil moisture change (ΔS_s) and the GMB (B), as shown in Eq. (17). The long-term GMB can be calculated according to Eq. (18). Because there is no permafrost in the KRB, it can be assumed that ΔS_s did not change. The contribution of the change in ice content in permafrost to the water balance is less than 1% on a yearly scale [40]. Precipitation was calculated by considering the precipitation gradient, E_s was simulated, and E_g was regarded as constant at 137.2 mm (Fig. 10c)[41]. Because there is no long-term observation of GMB in the KRB, we chose the two nearest glaciers (No. 1 in the headquarter of the Urumuqi river and Tuyuksu) in the Tianshan Mts., which have been observed in situ, to compare from 1959 to 2009. As can be seen from Table 4, the GMB value for Koxkar Glacier is between the values for the No. 1 and Tuyuksu glaciers, thus the simulated result is reasonable and credible. Glacial ablation in the KRB increased at a rate of 4.2 mm a^{-1} ($p < 0.01$) from 1959 to 2009, and the average elevation of glacier decreased by 18.53 m (16.68 m w.eq.), or at a rate of 370 mm a^{-1} (Fig. 10c).

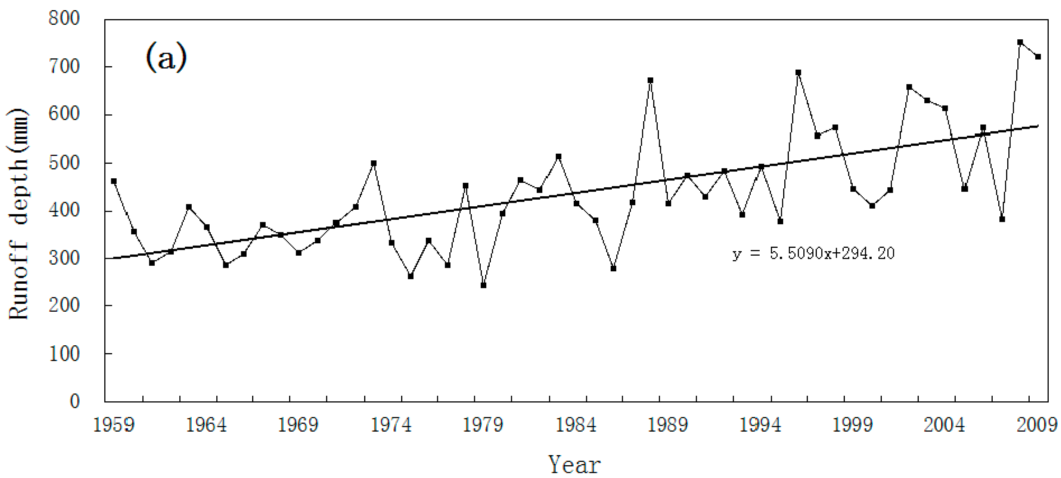

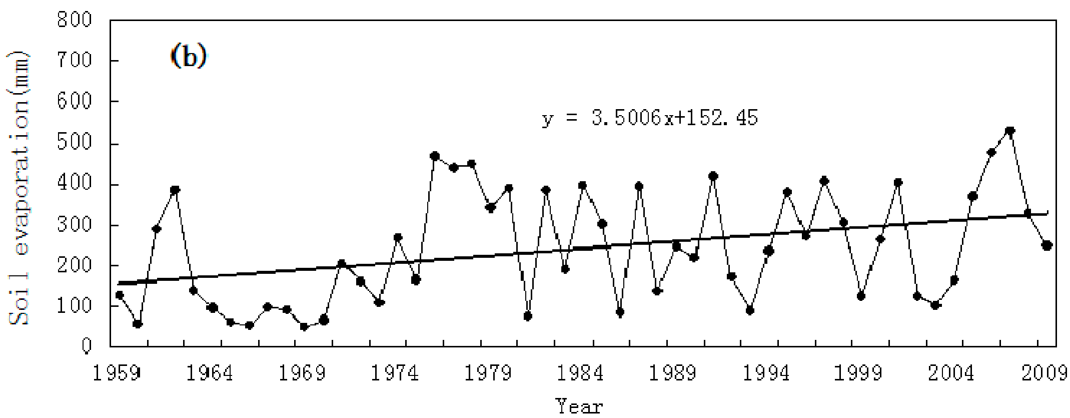

Preprints (www.preprints.org) | NOT PEER-REVIEWED | Posted: 31 October 2016 doi:10.20944/preprints201610.0139.v1

Peer-reviewed version available at Water 2017, 9, 100; doi:10.3390/w9020100

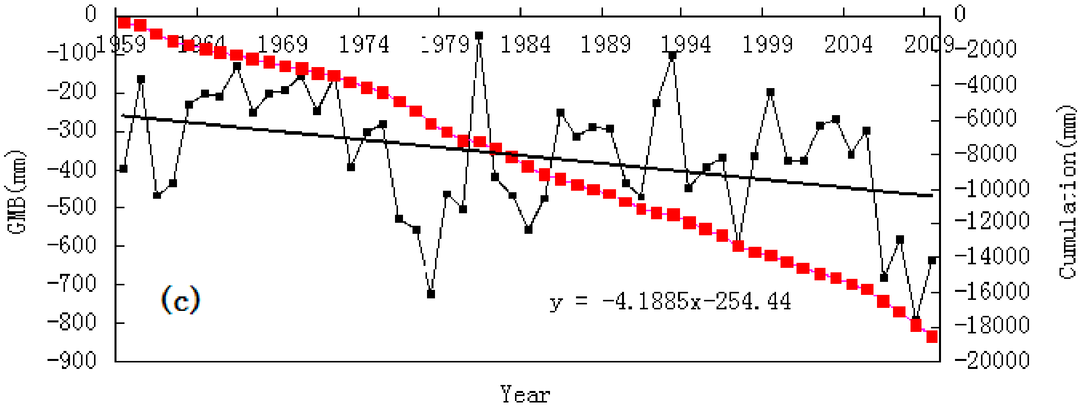

Fig. 10 Simulated annual runoff depth (a), evaporation (b), and annual glacier mass balance (GMB) and GMB (c) in the Koxkar river basin during 1959–2009

Table 4 Comparison of simulated and observed glacier mass balance accumulation between Koxkar Glacier and adjacent glaciers

Glacier	Koxkar (simulation)	No. 1 Glacier (Observation)	Tuyuksu Glacier (Observation)
1959-2009 Glacier mass balance accumulation	-18530 mm	-15200 mm	-20384 mm

5.3 Sensitivity analysis of runoff

In this study, we used the HBV model to analyze the sensitivity of runoff to changes of temperature and precipitation in the KRB. Climate change in the area is manifested mainly as changes in temperature and precipitation, and it has had a significant impact on the hydrological processes of the watershed, which is partly covered by glacier. Since the required input of the HBV model is daily data and the time interval of predicted meteorological data is monthly, in order to quantitatively study the sensitivity of runoff to changes in temperatures and precipitation, we assumed that the set of parameters and the glacier did not change into the future. Thus, the temperature was increased by 1℃, 2℃, and 4℃, respectively, the precipitation was increased by 10%, 20%, and 30%, respectively, and the runoff was simulated by the HBV model.

When the temperature was increased by 1℃ to 4℃, the amounts of change of monthly runoff differed, and the amount of annual runoff increased by 27.4%, 56.2%, 127%, respectively (Fig. 11, Table 5). As can be seen from Fig. 12, in the case of rising temperature, increases in the amount of runoff occur mainly from May to October. The month with the largest runoff is August, which shows that the runoff was supplied mainly by meltwater from the glacier. The distribution of internal annual runoff changes when temperature is higher (Fig. 11). Significantly increased runoff normally appears in May, and significantly decreased runoff normally appears in October; however, when temperature is higher, the significantly increased and decreased runoff shift to an earlier and later date, respectively.

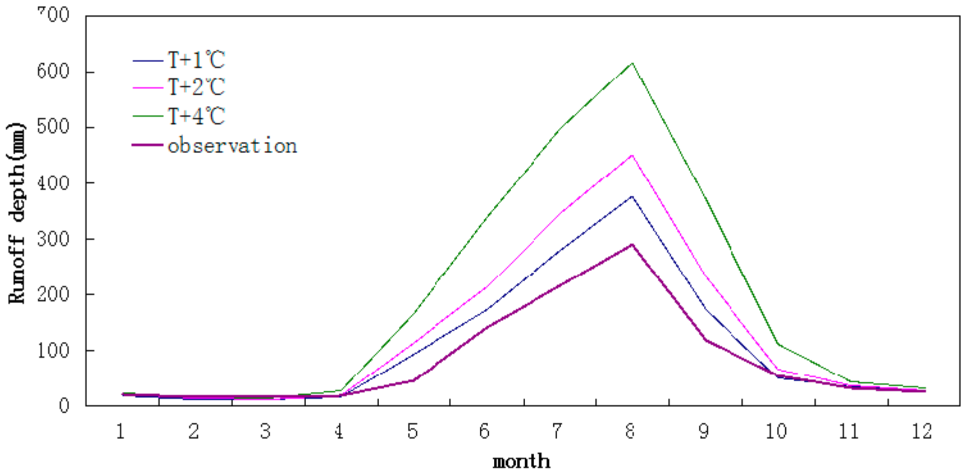

Fig. 11 Sensitivity of runoff under various temperature variations relative to 2007 to 2011

Table 5 Change of runoff under various changes of temperature

	T+1℃	**T+2℃**	**T+4℃**
Changes of runoff (%)	27.4	56.2	127.2

When precipitation increases by 10%, 20%, and 30%, monthly runoff increases by 6.1%, 11.3%, and 19.8%, respectively (Fig. 12, Table 6). Increased amounts of runoff occur mainly in the ablation season (from May to October). However, when precipitation is increased, the runoff does not increase very significantly. This is mainly because the runoff of Tianshan Mountain-based snowmelt is limited by temperature conditions; when only precipitation increases, runoff does not have a significant increase. Under the precipitation increases, increased runoff is concentrated mainly in June, July, and August. Within this period of time, radiation is sufficient and increased precipitation on the glacier leads to melting, which leads to increased runoff in the watershed. Increased precipitation causes a reduction in runoff from October to April (Fig. 12).

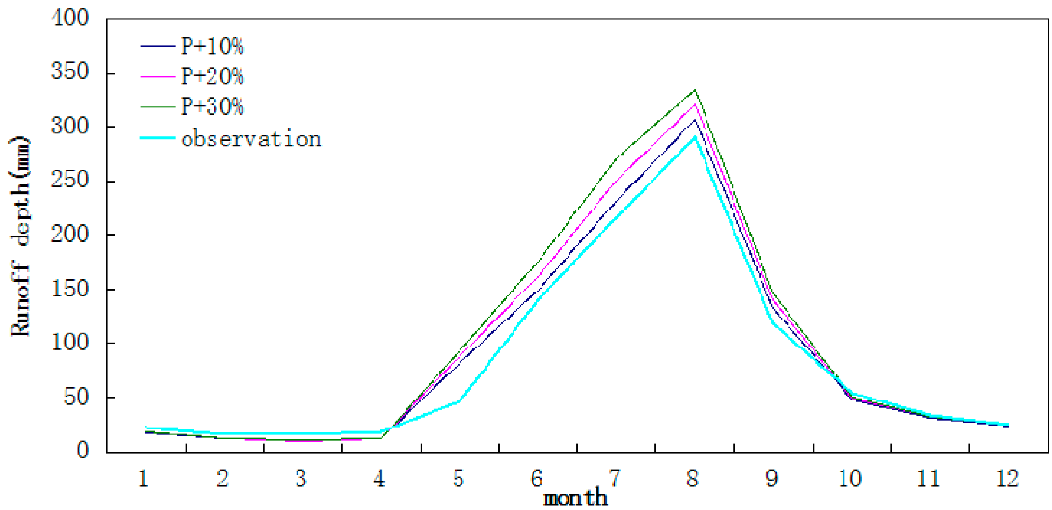

Fig. 12 Sensitivity of runoff under different precipitation variations relative to 2007 to 2011

Table 6 Change of runoff under various changes of precipitation

	P+10%	P+20%	P+30%
Change of runoff (%)	6.1	11.3	19.8

5.4 Discussion

Uncertainty of reconstructed meteorological data. Precipitation determines the accumulation of a glacier, and temperature determines the melting. Additionally, the amount and distribution of interannual variability of precipitation affects the supply and activity of a glacier [42]. In this study, we used polynomial regression and IDW based on gradients to reconstruct temperature and precipitation in the KRB from 1959 to 2009. The accuracy of the reconstructed temperature is higher than that of precipitation; this is mainly due to the temperature being influenced by single factors in the mountainous region [43]. The accuracy of the reconstructed monthly precipitation is better than that of daily precipitation. Precipitation in mountains is influenced by many factors, e.g., elevation, slope, aspect, surface conditions, etc. [44, 45]. We considered only the influence of elevation in this paper and did not consider other factors. However, although the interpolated accuracy of precipitation was influenced, the result can reflect the long-term trend of precipitation.

Temporal and spatial differences of gradients of temperature and precipitation. Gradients of precipitation and temperature are important input data for the HBV model, and these are fixed values in the model. However, gradients of precipitation and temperature have some differences under different altitudes and surface conditions [46]. Results show that the gradient of temperature has significant differences in areas of human activity, forest vegetation zones, and glaciated areas in each month, which can be up to 0.62℃ 100 m^{-1} at the same altitude in different months [47]. In the KRB, there are only six types of land cover and there is no human activity. Additionally, the area of glacier accounts for 76.9% of the watershed, so we assume that differences in surface conditions have little influence on the temperature gradient. In the Tianshan Mts., the gradient of precipitation is more complex than the gradient of temperature. Differences in lapse rate of precipitation are not only in a different aspect, but in a different aspect of the same month it is also significantly different, that is to say the gradient of precipitation of different month have differences in different elevation [45, 48]. Because of limitations from observation conditions, the gradients of precipitation and temperature in the KRB are averages, which makes the simulated process of runoff uncertain at the daily scale.

Temporal and spatial differences of degree-day factor. The degree-day factor of glacier and snow was an average value in the HBV model when we simulated runoff in the KRB. The degree-day factor is a key parameter in the degree-day model, and, with improved time resolution, the accuracy of the degree-day factor decreases [38]. The degree-day factor is a sensitive parameter in the HBV model when runoff in a watershed having glacier cover is simulated. It is influenced by temperature, altitude, slope, and aspect [49, 50]. Previous studies have indicated that the degree-day factor shows temporal and spatial differences in the Tianshan Mts. and Tibetan Plateau [19, 51, 52]. The area of the KRB is 116.7 km^2, and the value of degree-day factor is 9.5 mm/day.℃ in the model. Therefore, the monthly runoff is more accurate than the daily runoff, which was simulated by the HBV model. The trend of the GMB results is consistent with increased glacier ablation in the Tianshan Mts. and is reasonable and credible at the annual scale.

6. Conclusion

In this study, variations of runoff and glacial characteristics over the past 50 years were simulated and the sensitivities of runoff under different temperature and precipitation variations in the KRB were analyzed. Temperature and precipitation were found to increase by 0.32 °C $(10a)^{-1}$ and 4.8 mm a^{-1}, respectively, from 1959 to 2009 at Camp-AWS in the KRB. Runoff depth increased at 5.6 mm a^{-1}. The simulated GMB of the KG was approximately 370 mm a^{-1}. The glaciers thinned 18.53 m from 1959 to 2009. The runoff is more sensitive to variation of temperature than variation of precipitation. Increases in precipitation and temperature will lead to changes in the internal annual distribution of runoff.

Acknowledge: This study was supported by the National Key Program for Developing Basic Sciences in China (No. 2013CBA01806), the Chinese Academy of Sciences (KJZD-EW-G03-04), the National Natural Science Foundation of China (41501073, 41121001, 41271078), China Postdoctoral Science Foundation (2015M580893, 2016T90966). The authors would like to thank the Editors and the anonymous reviewers for their crucial comments, which improved the quality of this paper.

Author Contributions: Shichang Kang designed the experiments and revised the paper; Haidong Han contributed observed data; Min Xu run the model and worte the paper.

Conflict of Interest: No conflict of interest

Reference

1. Jansson, P.; Hock, R.; Schneider, T. The concept of glacier storage: a review. *J. Hydrol.* 2003, 282, 116-129.
2. Immerzeel, W. W.; van, Beek, L. P.; Bierkens, M. F. Climate Change Will Affect the Asian Water Towers. *Science*, 2010, 328, 1382-1385.
3. Li, J.; Liu, S.; Han, H.; Zhang, Y.; Wang, J.; Wei, J. Evaluation of runoff from Koxkar Glacier Basin, Tianshan Mountains, China. *Progress Inquisition Demutatione Climate*, 2012, 8, 357–363.
4. Giovanni, R.; Secondo, B.; Alessio, S.; Alfonso, S.; Marco, M. An integrated hydrological model for assessing climate change impacts on water resources of the Upper Po River Basin. *Water Resour. Manag*. 2015, 29, 1-23
5. Yang, Z. The Chinese Glacier Water Resource. Lanzhou: *Gansu science and Technology Press*, China, 1991, 137–148.
6. Li, K.; Li, Z.; Gao, W.; Wang, L. Recent East Tianshan glacier retreat and its impact on water resources. *Chin. Sci. Bull.* 2011, 56, 2708–2716.
7. Dombrowsky, I.; Hagemann, N.; Houdret, A. The river basin as a new scale for water governance in transition countries? A comparative study of Mongolia and Ukraine. *Environ. Earth Sci.* 2014, 72, 4705-4726.

8. Li, X. Study on Parameter Calibration and uncertainty Assessment of Hydrologic Model. Thesis of PhD, *Dalian University of Technology*, Dalian, 2005.
9. Lindstrom, G.; Harlin, J. Spill way design floods In Sweden—Applications and sensitivity analysis. Hydrol. Sci. J. 1992, 37, 521–539.
10. Liden, R.; Harlin, J. Analysis of conceptual rainfall-runoff modelling performance in different climates. *J. Hydrol.* 2000, 238, 231–247.
11. Gardelin, M.; Bergstrom, S.; Carlsson, B.; Graham, L. P.; Lindström, G. Climate change and water resources in Sweden—analysis of uncertainties. *Springer Netherlands*, 2006, 10, 189-207.
12. Menzel, L.; Burger, G. Climate change scenarios and runoff response in the Mulde catchment (Southern Elbe, Germany). *J. Hydrol.* 2002, 267, 53–64.
13. Hundecha, Y.; Bardossy, A. Modeling of the effect of land use changes on the runoff generation of a river basin through parameter regionalization of a watershed model. *J. Hydrol.* 2004, 292, 281–295.
14. Konz, M.; Uhlenbrook, S.; Braun, L.; Shrestha, A.; Demuth, S. Implementation of a process-based catchment model in a poorly gauged, highly glacierized Himalayan headwater. *Hydrol. Earth. Syst. Sci.* 2007, 11, 1323–1339.
15. Bergström, S.; Forsman, A. Development of a conceptual deterministic rainfall-runoff model. *Nord. Hydrol.* 1997, 3, 147–170.
16. Kang, E.; Cheng, G.; Lan, Y.; Zhang, J. Application of a conceptual hydrological model in the forecast of a mountain watershed. *Adv. Earth. Sci.* 2002, 17, 18–26.
17. Gao, H.; He, X.; Ye, B.; Pu, J. Modeling the runoff and glacier mass balance in a small watershed on the Central Tibetan Plateau, China, from 1955 to 2008. *Hydrol. Process.* 2012, 26, 1593-1603.
18. Xie, C.; Ding, Y.; Liu, S.; Han, H. Analysis on the glacial hydrological features of the glaciers on the south slope of Mt. Tuomuer and the effects on runoff. *Arid Land Geogr.* 2004, 27, 251–255.
19. Zhang, Y.; Liu, S.; Shangguan, D.; Xie, C.; Han, H.; Wang, J. Study of the positive degree-day factors on the Koxkar Baqi Glacier on the south slope of Tianshan Mountains. *J. Glaciol. Geocryol.* 2005, 27, 335–343.
20. Han, H.; Shao, J.; Lin, F.; Wang, J. Modeling the sensitivity of meltwater runoff of Tuomuer-type glacier to climate changes. *Progress Inquisition Demutatione Climate* 2012, 8, 357–363.
21. Wu, L. z.; Li, X. Dataset of the first glacier inventory in China. *Cold and Arid Regions Science Data Center*, Lanzhou, 2004, doi:10.3972/westdc.011.2013.db
22. Seibert J, Vis MJP (2012) Teaching hydrological modeling with a user-friendly catchment-runoff-model software package. *Hydrol. Earth. Syst. Sci. Discuss.* 2012, 16, 5905–5930.
23. Bergström, S.; Forsman, A. Development of a conceptual deterministic rainfall-runoff model. *Nord. Hydrol.* 1973, 3, 147–170.
24. Lang, H.; Musy, A. Hydrology in mountainous regions. *IAHS Publ.* Wallingford, 1990, 99–106.
25. Young, G. J. Snow and glacier hydrology, Proceedings of the Kathmandu of an international symposium. *IAHS Publ,* Wallingford, 1992, 249–260.
26. Seibert, J. Dissertation, 1999.
27. Braithwaite, R. J.; Olesen, O. B. Ice ablation in West Greenland in relation to air temperature. *Zeitschrift Für Gletscherkunde Und Glazialgeologie* 1984, 20, 155–168.
28. Fountain, A. G.; Tangborn, W. V. The effect of glaciers on streamflow variations. *Water Resour. Manag.* 1985, 21, 579–586.
29. Fujita, K.; Seko, K.; Ageta, Y.; Pu, J. C.; Yao, T. D. Superimposed ice in glacier mass balance on the Tibetan Plateau. *J. Glaciol.* 1996, 42, 454–460.

30. Fujita, K.; Ohta, T.; Ageta, Y. Characteristics and climatic sensitivities of runoff from a cold-type glacier on the Tibetan Plateau. *Hydrol. Process.* 2007, 21, 2882–2891.
31. Bergström, S. The HBV-Model—its structure and applications. *SMHI (Swedish Meteorological and Hydrological Institute) Reports Hydrology*, 1992, 4, 32.
32. Seibert, J. HBV manual, 2005.
33. Nash, J. E.; Sutcliffe, J. V. River flow forecasting through conceptual models, Part Ⅰ - a discussion of principles. *J. Hydrol.* 1997, 10, 282–290.
34. Zhao, G.; Yang, T.; Tian, H. Response of glacier area variation to climate change in southern Tianshan Mountains during 1990–2011. *Res. Soil Water Conserv.* 2014, 21, 257–268.
35. Hornberger, G. M.; Cosby, B. J.; Galloway, J. N. Modelling the effect of acid deposition: Uncertainty and spatial variability in estimation of long-term sulphate dynamics in a region. *Water Resour. Manag.* 1986, 22, 1293–1302.
36. Seibert, J. Estimation of parameter uncertainty in the HBV Model. *Hydrol. Res.* 1997, 28, 247–262.
37. Uhlenbrook, S.; Seibert, J.; Leibundgut, C.; Rodhe, A. Prediction uncertainty of conceptual rainfall-runoff models caused by problems in identifying model parameters and structure. *Hydrol. Sci. J.* 1999, 44, 779–797.
38. Hock, R. Temperature index melt modelling in mountain areas. *J. Hydrol.* 2003 282, 104–115.
39. Sun, M.; Li, Z.; Yao, X.; Zhang, M. Analysis on runoff variation of Glacier No. 1 at the headwaters of the Urumqi River from 1959 to 2008. *J. Nat. Resour.* 2012, 27, 650–660.
40. Zhang, Y. S. Hydrological processes and their features. In: Dynamic features of cryosphere in the middle of Qinghai-Tibet Plateau. *Geological Press*, Beijing, 2002, 199–206.
41. Zhang, Y.; Yao, T.; Pu, J. The features of hydrological processes in the Dongkemadi River Basin, Tanggula Pass, Tibetan Plateau. *J. Glaciol. Geocryol.* 1997, 18, 214–222.
42. Zhang, X.; Yang, Z. The primary analysis of water-balance in Binggou Basin of Qilian Mountains. *J. Glaciol. Geocryol.* 1991, 13, 35–42.
43. Rolland, C. Spatial and seasonal variations of air temperature lapse rates in Alpine regions. *J Climate*, 2003, 16, 1032–1046.
44. Wang, N.; He, J.; Jiang, X.; Song, G.; Pu, J.; Wu, X.; Chen, L. Study on the zone of maximum precipitation in the north slope of the central Qilian Mountains. *J. Glaciol. Geocryol.* 2009, 31, 395–403.
45. Mu, Z.; Jiang, H. The vertical distribution law of precipitation in the western Tianshan Mountain based on TRMM/TMI. *J. Arid Land Resour. Environ.* 2010, 24, 66–71.
46. Shi, Y. Glaciers and related environments in China. *Science Press*, Beijing, 2000, 80-86.
47. Xin, H.; He, Y.; Li, Z.; Wang, S.; Du, J.; Wang, C.; Pu, T.; Zhang, W. Inter-annual variation of temperature and precipitation gradient at the eastern slope of Yulong Snow Mountain. *Earth Science-J. China U. Geosci.* 37, Suppl, 2012, 188–194.
48. Liu, J.; Cheng, R.; Qin, W.; Yang, Y. Study on the vertical distribution of precipitation in mountainous regions using TRMM data. *Adv. Water Sci.* 2011, 22, 447–454.
49. Braithwaite, R. J.; Zhang, Y. Sensitivity of mass balance of five Swiss glaciers to temperature changes assessed by tuning a degree-day model. *J. Glaciol.* 2000, 152, 7–14.
50. Singh, P.; Kumar, N.; Arora, M. Degree-day factors for snow and ice for Dokriani Glacier, Garhwal Himalayas. *J. Hydrol.* 2000, 235, 1–11.

51. Qiao, C.; He, X.; Ye, B. Study of the degree-day factors for snow and ice on the Dongkemadi Glacier, Tanggula Range. *J. Glaciol. Geocryol.* 2010, 32, 257–264.

52. Wu, Q.; Kang, S.; Gao, T.; Zhang, Y. The characteristics of the positive degree-day factors of the Zhadang Glacier on the Nyainqentanglha Range of Tibet Plateau, and its application. *J. Glaciol. Geocryol.* 2010, 32, 257–264.